A Leidenfrost Point Model for Impinging Droplets and Sprays

John D. Bernardin
International, Space, and Response Division,
Los Alamos National Laboratory,
P.O. Box 1663, MS D466,
Los Alamos, NM 87545

Issam Mudawar
Boiling and Two-phase Flow Laboratory,
School of Mechanical Engineering,
Purdue University,
West Lafayette, IN 47907

This study presents, for impinging droplets and sprays, a model of the Leidenfrost point (LFP); the minimum liquid/solid interface temperature required to support film boiling on a smooth surface. The present model is an extension of a previously developed sessile drop model, based on bubble nucleation, growth, and merging criteria, as well as surface cavity size characterization [3]. The basic concept of the model is that for liquid/solid interface temperatures at and above the LFP, a sufficient number of cavities are activated and the bubble growth rates are sufficiently fast that a continuous vapor layer is established nearly instantaneously between the liquid and the solid. For impinging droplets, the influence of the rise in interfacial pressure created by the impact of the droplet with the surface, must be accounted for in determining fluid properties at the liquid-solid interface. The effect of droplet impact velocity on the LFP predicted by the model is verified for single impinging droplets, streams of droplets, as well as sprays. While the model was developed for smooth surfaces on which the roughness asperities are of the same magnitude as the cavity radii (0.1–1.0 μm), it is capable of predicting the boundary or limiting Leidenfrost temperature for rougher surfaces with good accuracy.
[DOI: 10.1115/1.1652045]

Keywords: Boiling, Droplet, Heat Transfer, Impingement, Phase Change, Sprays

Introduction

Material processing leaders are under constant pressure to improve the material and performance characteristics of products, while at the same time, increase the efficiency of the processing techniques by reducing energy consumption, scrap material, and manufacturing time. For example, the needs for stronger, lighter, and cheaper materials in the automobile, railroad, and aerospace industries, have driven improvements in the processing of aluminum alloys. In particular, advances in heat treatment and forming operations have led to alloys with improved strength-to-weight ratios and enhanced corrosion resistance properties. However, lack of understanding scientific principles in several areas still leads to inefficient manufacturing cycles with large numbers of scrap parts and long production periods. One of the least understood areas of materials processing involves quenching, or the rapid cooling of a part, such as that which occurs following an extrusion, casting, forging, or heat treating operation. When done correctly, quenching can result in high performance parts. However, when performed incorrectly, quenching can result in parts with poor or nonuniform material properties, high residual stresses, and severe distortion.

One common method of quenching involves immersing the heated part in a deluge of water sprays. The spray quenching method is often preferred over bath immersion quenching, as the former can produce much higher heat transfer rates and more uniform or controlled temperature fields within the part. Figure 1 shows a typical temperature-time history of a part during a spray quench. The quench curve is divided into four distinct regimes, each possessing particular heat transfer characteristics. In the high temperature, or film boiling regime, the quench proceeds rather slowly as liquid-solid contact is minimized by the rapid formation of an insulating vapor blanket at the droplet-solid interface. In this regime, the droplets appear to shatter and bounce off of the solid surface upon contact. The lower temperature boundary of this regime is referred to as the Leidenfrost point (LFP). As surface temperatures drop below the LFP, a transition boiling regime is encountered, where partial and prolonged liquid-solid contact occurs and the cooling rates increase. Further cooling brings about the nucleate boiling regime, where complete wetting of the surface occurs and the heat transfer rates are the highest as vigorous vapor generation occurs as the droplets spread out on the solid surface. At the bottom end of the nucleate boiling regime, boiling ceases and the single-phase heat transfer regime is encountered, where heat transfer is dominated by single-phase convection.

As discussed in [1], during the quench phase of a heat treatment operation involving aluminum alloys, most of the material transformations occur at temperatures above the LFP, while warping and distortion, caused by thermal stresses generated by large cooling rates, take place at temperatures below the LFP. Consequently, accurate knowledge of the Leidenfrost temperature and the parameters that govern its behavior is paramount to controlling the quenching process and subsequent material properties.

In a previous investigation by the authors [2], an extensive experimental sessile droplet LFP database was developed and used to assess several existing LFP models. These assessments indicated that the previously developed LFP models were lacking in their ability to accurately and consistently predict the LFP for a variety of fluid and surface conditions. From that experimental study [2], Bernardin and Mudawar [3] developed a new LFP model for sessile droplets, based on surface cavity characterization as well as bubble nucleation, growth, and interaction criteria. The premise for that model was that as the Leidenfrost temperature is approached from the boiling incipience temperature, smaller and more numerous surface cavities become activated, and the growth rate of these bubbles increases appreciably. For liquid-solid interface temperatures at and above the LFP, a sufficient number of cavities are activated and the bubble growth rates are large enough that liquid in immediate vicinity of the surface is nearly instantaneously converted to vapor upon contact. These two features enable a continuous insulating vapor layer to form between the liquid and the solid.

The focus of the study reported here was to take the existing sessile drop LFP model [3] and extend its application to impinging drops and sprays. The main features of the previous sessile drop LFP model, as well as the additional concepts needed to extend the model to impinging drops, will be presented below.

Contributed by the Heat Transfer Division for publication in the JOURNAL OF HEAT TRANSFER. Manuscript received by the Heat Transfer Division April 9, 2003; revision received December 4, 2003. Associate Editor: R. M. Manglik.

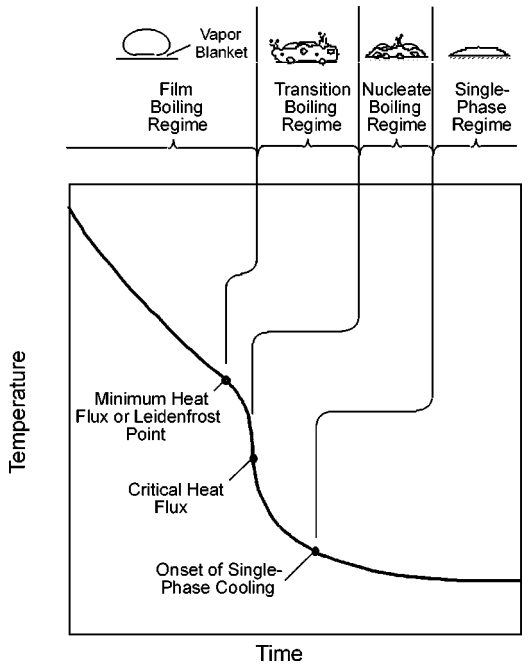

Fig. 1 Typical temperature-time history of a surface during spray quenching

The successful application of the extended LFP model will be demonstrated by a comparison between predicted and measured Leidenfrost temperatures for drops and sprays.

Leidenfrost Point Model Development

The methodology used to construct the LFP model is based on two aspects concerning bubble nucleation and its relationship to surface temperature and cavity shape and distribution. First, raising surface superheat beyond the boiling incipience temperature results in the activation of both larger and smaller surface cavities and an increase in the bubble growth rates. Secondly, for a typical polished surface, there is an exponential increase in the number of surface cavities with decreasing cavity mouth radius [4,5].

In the previous study by Bernardin and Mudawar [3], the authors postulated that at some large liquid-solid interface temperature corresponding to the LFP, a sufficient number of cavities would activate to produce enough vapor to completely separate the liquid from the solid, and hence, induce film boiling. Discussed below are the various sub-models used to support the overall LFP model for impinging droplets. In the next section, a solution procedure based upon these sub-models is outlined.

Bubble Nucleation. The first part of the LFP model involves the criteria for bubble nucleation from surface cavities as a liquid comes into contact with a solid surface. The minimum condition necessary for bubble nucleation is met when the available superheat, T_{ash}, in the liquid at a distance y from the solid surface, is equal to the required nucleation superheat, T_{rsh}, for a hemispherical bubble whose radius, r, is equal to y. This condition, as it applies to the transient condition when a liquid contacts a surface, is represented by

$$T_{sat}\exp\left(\frac{2\sigma v_{fg}}{rh_{fg}}\right)=T_i+(T_f-T_i)\mathrm{erf}\left(\frac{r}{2\sqrt{\alpha_f t}}\right) \tag{1}$$

where t is the time following liquid-solid contact and T_i is the liquid-solid interface temperature defined by

$$T_i=\frac{(k\rho c_p)_s^{0.5}T_s+(k\rho c_p)_f^{0.5}T_f}{(k\rho c_p)_s^{0.5}+(k\rho c_p)_f^{0.5}} \tag{2}$$

where T_s and T_f are, respectively, the surface and liquid temperatures prior to the contact. More details concerning this sub-model development can be found in [3].

Cavity Size Distribution. The second sub-model involves the surface cavity size distribution. Surface cavities and other defects, typically on the order of 1 to 10 μm, have long been known to be highly influential in controlling nucleate boiling by serving as nucleation sites.

In a previous study by the authors [3], scanning electron microscopy (SEM) was utilized to characterize the surface cavity distributions of macroscopically polished surfaces from which empirical Leidenfrost temperature measurements were made. From inspection of various SEM images at different magnifications, it was apparent that the number of cavities per unit area, n, having an equivalent mouth radius between r and $r+\Delta r$, could be fit by the exponential function

$$n=a_1\exp(-a_2 r) \tag{3}$$

Using the scanning electron microscopy images of the various surfaces from that study, the following curve fits were obtained over a cavity size range of 0.07 to 1.0 μm

$$n=3.379\exp(-10.12r)\quad(\text{aluminum}) \tag{4a}$$

$$n=4.597\exp(-12.20r)\quad(\text{nickel}) \tag{4b}$$

$$n=13.16\exp(-16.07r)\quad(\text{silver}), \tag{4c}$$

where the units for n and r are sites-μm^{-2}-μm^{-1} and μm, respectively. The curve fits had acceptable least square residuals greater than 0.9.

The cumulative number of surface cavities in the radius interval $r_{\min}\leqslant r\leqslant r_{\max}$, is then obtained through integration,

$$nc=\int_{r_{\min}}^{r_{\max}}n(r)dr=\frac{a_1}{a_2}[\exp(-a_2 r_{\min})-\exp(-a_2 r_{\max})] \tag{5}$$

Bubble Growth. The third sub-model is related to the bubble growth that occurs from activated cavities. Due to the relatively high superheat and short duration over which vapor is created in the film boiling regime, it is believed the rapid bubble growth is initially dominated by inertia rather than heat diffusion. For this condition, bubble growth is described by the Rayleigh equation (neglecting viscous effects) which can be derived from the momentum equation for incompressible and irrotational flow [6], or from energy conservation principles [7], incorporating the pressure drop across a spherical interface, $2\sigma/R$.

$$R\ddot{R}+\frac{3}{2}\dot{R}^2=\frac{1}{\rho_f}\left[(P_g-P_\infty)-\frac{2\sigma}{R}\right], \tag{6}$$

where $\dot{R}$ and $\ddot{R}$ are, respectively, the first and second derivatives of bubble radius with respect to time, and P_∞ is the liquid pressure far from the bubble interface.

In solving the Rayleigh equation, the following intermediate substitutions were performed:

$$\left[R\ddot{R}+\frac{3}{2}\dot{R}^2\right]R^{1/2}=\frac{d(R^{3/2}\dot{R})}{dt} \tag{7}$$

and

$$\frac{R^{1/2}}{\rho_f}\left[\Delta P-\frac{2\sigma}{R}\right]=\frac{1}{R^{3/2}\dot{R}}\frac{d}{dt}\left[\frac{\Delta P R^3}{3\rho_f}-\frac{\sigma R^2}{\rho_f}\right] \tag{8}$$

where $\Delta P=(P_g-P_\infty)$.

Substituting Eqs. (7) and (8) into Eq. (6) and performing the integration leads to the following integral:

$$t = \int_0^R \frac{dR}{\left[\frac{2\Delta P}{3\rho_f} - \frac{2\sigma}{\rho_f R}\right]^{0.5}}, \quad (9)$$

which can be solved by numerical techniques [3,8].

This model development assumed that the bubbles have a hemispherical shape and that the effect of viscosity could be neglected. Previous empirical studies [9–11] revealed that nucleating bubbles were generally hemispherical or near-spherical in shape. Furthermore, Johnson et al. [11] and Carey [12] both indicated that for rapid bubble growth, like that experienced near the Leidenfrost point, the inertial forces dominate and the bubbles have a hemispherical shape. Finally, previous analytical bubble growth models [7,10,13,14] that employed spherical bubble shapes and neglected the effect of viscosity, proved to be very accurate when compared to empirical bubble growth rate measurements.

Interaction of the Thermal Boundary Layer and the Growing Bubbles. The growth rate of a bubble, as predicted by the numerical solution to the Rayleigh equation, is several orders of magnitude faster than that of the thermal boundary layer (right-hand side of Eq. (1)). Therefore, it is assumed the early stage of bubble growth is described by the solution to Eq. (9) until the bubble dome reaches the maximum bubble stability point in the growing thermal boundary layer predicted by Eq. (1), after which the bubble growth is controlled by this slower diffusion rate of the thermal boundary layer.

As individual bubbles grow, they begin to merge and form a vapor layer. The formation of this vapor layer is influenced by a number of factors including entrainment of vapor within cavities, merging of bubbles, and cancellation of nucleation sites by growing bubbles. All of these factors serve to decrease the number of bubble nucleation sites participating in the growth of the vapor layer at the liquid-solid interface. More details and experimental observations of these factors, including the influence of these parameters in the prediction of the LFP, can be found in [3].

Influence of Droplet Impact Velocity. The approach for determining the Leidenfrost temperature for impinging droplets is identical to that for sessile droplets with the exception that the impact pressure must be correctly modeled when determining fluid properties at the liquid-solid interface. When a droplet impinges perpendicularly upon a rigid surface, the pressure rise at the liquid-solid interface at the moment of impact is significantly higher than the increase in stagnation pressure, $0.5\ \rho_f\ u_o^2$, because of compressibility effects. The most frequently used approximations to the pressure increase which develops during droplet impact are based upon one-dimensional elastic impact theory [15]. This theory states that the interfacial pressure increase that results when two elastic media collide, assuming Hooke's law is valid, is given by the solution to the one-dimensional longitudinal wave equation [16]:

$$\Delta P = \rho_f u_o u_{snd} \quad (10)$$

where u_o is the droplet impact velocity and u_{snd} is the speed of sound in the liquid.

Labeish [17] claimed that Eq. (10) could be applied to impinging droplets to predict the impact pressure. Engel [18], however, performed an analysis which accounted for droplet curvature and the transient impact behavior, concluding Eq. (10) overpredicts the impact pressure and must be multiplied by a correction factor, given as 0.20 for water on various solids including aluminum and copper [19].

Based upon Engel's findings [18,19], the following 20 percent elastic impact pressure relation was used in the present study to predict the pressure at the liquid-solid interface during the impact:

$$\Delta P = 0.20 \rho_f u_o u_{snd} \quad (11)$$

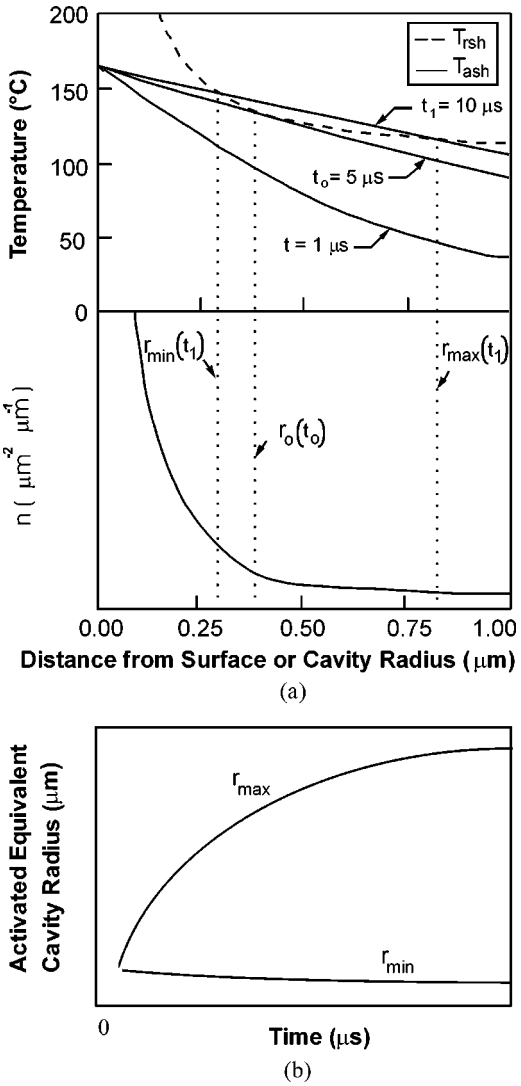

Fig. 2 Transient cavity nucleation model including (*a*) cavity nucleation superheat criteria and corresponding cavity size distribution with transient activation window, and (*b*) transient maximum and minimum active cavity radii for water in contact with a hot surface with an interface temperature of 165°C [3]

Leidenfrost Model Solution Procedure

To perform the LFP model solution procedure for impinging droplets, the pressure increase must first be determined with Eq. (11) so that fluid properties in the vicinity of the liquid-solid interface can be accurately determined.

Next, the surface cavity activation and bubble growth process must be modeled. To achieve this step, one must understand the thermal processes taking place during the initial impact of the droplet. Upon contact between an impinging droplet and a heated surface, a thermal boundary layer begins to develop in the liquid, as displayed in Fig. 2(*a*) for a water droplet in contact with a hot surface at 165°C. At some time t_o, the thermal boundary layer has grown sufficiently large such that the available superheat, T_{ash}, is equal to the required superheat, T_{rsh}, needed to satisfy the bubble nucleation criterion for conical-shaped cavities with a mouth radius r_o, (Eq. (1)), as shown in Fig. 2(*a*). For a polished surface, this radius is typically well within the range of cavity radii available on the surface. As time progresses and thermal boundary layer thickens, all cavities within a specific cavity radius interval are activated. This interval is given by the two roots of Eq. (1), namely, $r_{\min}(t)$ and $r_{\max}(t)$, as displayed in Fig. 2(*b*), where $r_{\max}$ is

the radius of the largest activated cavity at a given instant, not the largest cavity on the surface. Similarly, $r_{\min}$ is the smallest activated cavity.

Assuming only a fraction, ψ, of the cavities actively participate in the growth of the vapor layer due to the cancellation effects described in the previous section, and that bubbles grow from cavities as hemispheres, the time dependence of the cumulative number of activated cavities per unit area, nc_a, can be found by integrating the cavity size distribution, Eq. (3), over the active cavity radius limits $r_{\min}(t)$ and $r_{\max}(t)$:

$$nc_a(t)=\psi\int_{r_{\min}(t)}^{r_{\max}(t)} a_1\exp(-a_2 r)dr=\psi\frac{a_1}{a_2}\{\exp(-a_2 r_{\min}(t))-\exp(-a_2 r_{\max}(t))\}. \quad (12)$$

Since the inertia-controlled bubble growth rate predicted by Eq. (9) is orders of magnitude greater than the thermal boundary layer growth rate, it is assumed all bubbles initiated with $r_o<r_{\max}(t)$ will rapidly grow to $r_{\max}(t)$, the maximum stable hemispherical bubble radius supported by the growing thermal boundary layer. A hemispherical bubble will not be stable for sizes beyond $r_{\max}(t)$ as condensation on the leading front of the growing bubble would significantly reduce its growth rate [20]. This is consistent with bubble incipience model of Hsu [21] and the experimental results of Clark et al. [22]. Consequently, the limiting condition considered here is that once the bubbles reach the thermal boundary layer limit of $r_{\max}(t)$ they will continue to grow at the same rate as the thermal boundary layer, i.e., $\dot{r}_{\max}(t)$. This two-stage growth is consistent with the bubble growth findings of Lee and Merte [13].

Given this bubble growth model, the time-dependent percent area coverage of the liquid-solid interface by vapor, $AB\%(t)$, is then given by

$$AB\%(t)=nc_a(t)\pi r_{\max}^2(t)\times 100\% \quad (\%) \quad (13)$$

which, upon substitution of Eq. (12), gives

$$AB\%(t)=\psi\frac{a_1}{a_2}\times\{\exp(-a_2 r_{\min}(t))-\exp(-a_2 r_{\max}(t))\}\pi r_{\max}^2(t)\times 100\% \quad (\%) \quad (14)$$

where a_1 and a_2 are experimentally determined constants, such as those given in Eqs. (4*a*) through (4*c*).

Bernardin and Mudawar [3] used experimental evidence to arrive at a value of 0.05 for the cavity cancellation parameter, ψ. As Bernardin and Mudawar discuss, the present models for surface characterization and bubble nucleation are limited in their degree of accuracy and a more accurate means of determining the percent of actively participating surface cavities, ψ, is currently unavailable and warrants further investigation. Nevertheless, it should be emphasized that while the choice of ψ will influence the vapor layer growth rate, the strong temperature-dependence of the latter, $\Delta AB\%/\Delta t$, which is used to identify the LFP in the present model, is still very well preserved.

Shown in Fig. 3(*a*) is the temperature dependence of the transient vapor layer growth for a sessile water droplet on a polished aluminum surface with a cavity distribution given by Eq. (4*a*), as determined in the previous study by Bernardin and Mudawar [3]. The time for complete vapor layer development ($AB\%=100$) is shown to rapidly decrease as the interface temperature is increased from 145 to 185°C. While the model predicts an eventual 100% vapor layer growth for the interface temperature of 145°C, other effects such as bubble departure and liquid motion which are not accounted for in the model, would interrupt this development within a few milliseconds of liquid-solid contact, and hence prevent film boiling from occurring. Figure 3(*b*) displays the vapor layer growth rate, $\Delta AB\%/\Delta t$ or average slope of the curves in Fig. 3(*a*), as a function of the liquid-solid interface temperature. Figure 3(*b*) shows that as the interface temperature increases beyond the liquid saturation temperature, the average vapor layer

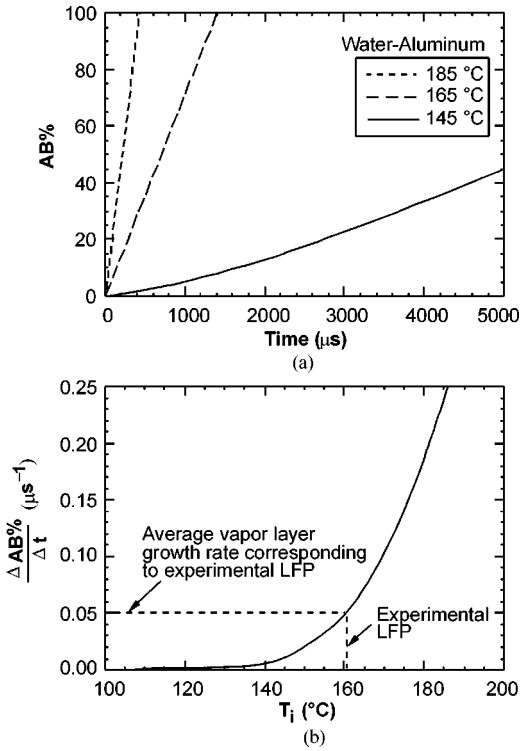

Fig. 3 Temperature dependence of the (*a*) transient vapor layer coverage and (*b*) average vapor layer growth rate for a sessile water droplet on a polished aluminum surface [3]

growth rate increases exponentially. Intuition suggests that at some minimum interface temperature, the LFP, the average vapor layer growth rate will become sufficiently high to support film boiling.

To determine the minimum average vapor layer growth rate required to support film boiling, experimental LFP data for sessile water droplets on aluminum were employed [2]. Shown in Fig. 3(*b*) is the experimentally determined Leidenfrost temperature of 162°C ($T_s=170$°C) for sessile water droplets on aluminum, which corresponds to an average vapor layer growth rate of 0.05 μs^{-1}. Note that the experimentally measured Leidenfrost temperature had an uncertainty of ±5°C [2]. Bernardin and Mudawar [3] employed this value of the average vapor layer growth rate to accurately identify the LFP for a sessile drop in a variety of liquid-solid systems. This same technique, as described by Carey [12], has been used to determine the critical vapor bubble formation rate needed to sustain homogeneous nucleation within a superheated liquid. In the homogeneous nucleation superheat limit model, the vapor bubble formation rate increases exponentially with increasing liquid temperature, much like the vapor blanket growth rate in the present study. Carey explains how empirical data were used to determine a critical vapor bubble formation rate, and how this single bubble formation rate was used to determine the homogeneous nucleation superheat limit of several different liquids including water.

Consequently, this average vapor growth rate of 0.05 μs^{-1} is used in the present study to identify the LFP for impinging droplets.

While this modeling process was presented for a single impinging droplet, it can also be used to predict the LFP for a spray. To predict the local LFP for a spray, the mean droplet velocity of the spray in the area of interest should be used in Eq. (11) to determine the average droplet impact pressure. The remaining modeling procedure is identical to that outlined above for a single droplet.

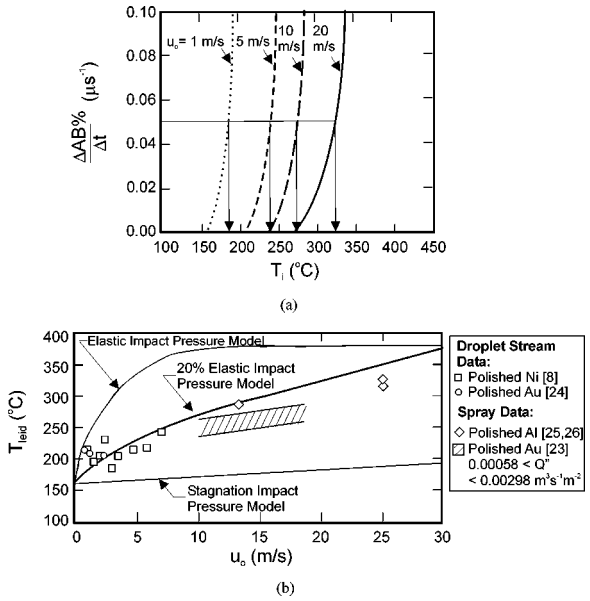

Fig. 4 (*a*) Velocity and temperature dependence of the average vapor layer growth rate for water droplets impinging upon a polished aluminum surface, and (*b*) comparison of the velocity dependent LFP model for water droplets impinging upon a polished surface, using different impact pressure sub-models, with experimental data. The uncertainties of experimental Leidenfrost temperatures and droplet impact velocities measured in studies [8,23–26] were reported not to exceed ±10°C and ±0.5 m/s, respectively.

Leidenfrost Model Assessment

Figure 4(*a*) displays the average vapor layer growth rate versus interface temperature for water droplets impinging at different velocities upon a polished aluminum surface. For the four different droplet velocities, the fluid properties were evaluated with the 20% elastic impact pressure relation given by Eq. (11). Using an average vapor layer growth rate of 0.05 μs^{-1}, the Leidenfrost temperatures corresponding to the various droplet velocities were determined. The following expression relating the Leidenfrost temperature to the water droplet velocity was determined from the data in Fig. 4(*a*):

$$T_{\text{leid}} = 162.0 + 24.3u_o^{0.64} \quad (^\circ\text{C}) \tag{15}$$

where the units on u_o are m s^{-1}. Equation (15) is displayed in Fig. 4(*b*), and is labeled with ''20 percent Elastic Impact Pressure Model,'' indicating that Eq. (11) was used in its development. Also displayed in Fig. 4(*b*) are the LFP predictions that would be obtained if the full elastic or stagnation impact pressure sub-models were used in place of Eq. (11) to determine the fluid properties. While Eq. (15), and the LFP model for that matter, does not explicitly give an upper temperature bound for the LFP, a maximum temperature limit does exist. The maximum temperature that a liquid can be heated to, above which it is nearly instantaneously converted to vapor, is referred to as the kinetic or thermodynamic superheat limit. Techniques for predicting this superheat limit can be found in [12]. Further details on the superheat limit for water and its relationship to the present LFP model can be found in [3].

To assess the accuracy of the LFP model for impinging droplets, experimental LFP data for single water droplet streams and sprays are included in Fig. 4(*b*). The shaded band representing the empirical LFP spray correlation of Klinzing et al. [23] covers the range of volumetric spray fluxes ($0.00058 < Q'' < 0.00298\ \text{m}^3\,\text{s}^{-1}\,\text{m}^{-2}$) used in that study. Although the experimental data used in the comparison correspond to different surface material types, the surface preparation for each was similar. Thus, the cavity size distributions and Leidenfrost temperatures for the various surface materials are expected to be fairly similar, as was found previously by Bernardin and Mudawar [3] for polished aluminum, nickel, and silver surfaces. The comparison in Fig. 4(*b*) indicates that the LFP models generated with either the full elastic impact or the stagnation impact pressure sub-models, yield significant deviations between the predictions and the empirical data. In contrast, the LFP model that used the 20 percent elastic impact pressure sub-model, agrees quite well with the experimental data. In most cases, the model lies within the experimental data's error bands of ±10°C in temperature and ±0.5 m/s in droplet velocity. In addition, the impinging water drop LFP model given by Eq. (15), predicts a Leidenfrost temperature of 162.0°C for a sessile water drop ($u_o = 0.0\ \text{m s}^{-1}$), which is in agreement with the sessile drop LFP model prediction [3] and the experimentally measured value [2] for water on polished aluminum.

Differences between the LFP model predictions and experimental Leidenfrost temperature data may be attributed to a number of factors. First, the surface cavity size distribution, *nc*, and cavity cancellation parameter, ψ, used to arrive at Eq. (15), were taken from a study of water droplets on a polished aluminum surface [3], whereas the experimental LFP data of Fig. 4 came from studies using a variety of polished metal surfaces. A more accurate determination of Eq. (15) using a cavity size distribution for each particular surface may yield better agreement between the Leidenfrost temperature predictions and measurements. Further investigation of the cavity cancellation parameter is also warranted, as its value is dependent on the droplet fluid properties and solid surface finish [3].

The 20 percent elastic impact model may be a source of some uncertainty as well. This model, represented by Eq. (11), does not account for break-up of the impacting droplet and its subsequent influence on the impact pressure. The stability of the spreading droplet film has been observed in numerous empirical studies to be a function of, in part, droplet velocity and surface roughness, as summarized in [24]. Hence, by more accurately accounting for the effects of droplet velocity and surface roughness on the impact pressure, a better prediction of the Leidenfrost temperature of impinging drops may be obtained.

While some uncertainties do exist in the development of the present LFP model, Eq. (15) and Fig. 4(*b*) reveal the dependence of the LFP on droplet velocity, something that previous LFP models have failed to accomplish [2]. As Fig. 4(*b*) indicates, the Leidenfrost temperature for an impinging droplet or spray can be significantly higher than that predicted for a sessile droplet. Consequently, the present LFP model should prove beneficial in predicting and controlling the spray heat transfer process encountered in materials processing and other applications.

Application to Rough Surfaces. While the present model was developed for polished surfaces, it also provides a limiting condition for surfaces possessing roughness features orders of magnitude larger than the cavity radii responsible for bubble nucleation (0.1 to 1 μm). As discussed earlier, surface contamination and roughness promotes and enhances the shattering of droplets upon impact [24]. Consequently, rough surfaces would expect to have a lower interfacial impact pressure and a corresponding lower Leidenfrost temperature when compared to a polished surface. Figure 5 shows experimentally measured Leidenfrost temperatures for water droplets of different velocities, impinging upon polished and particle blasted surfaces. For each droplet velocity studied, the Leidenfrost temperature for the polished surface was consistently higher than that for the particle blasted surface. In addition, the measured Leidenfrost temperature for the particle blasted surface, for the most part, was lower than the LFP model prediction. Consequently, the LFP model outlined in this study appears to predict an upper limit to the Leidenfrost temperature for droplets impinging upon rough surfaces. The complex relationship between surface roughness, droplet impact stability,

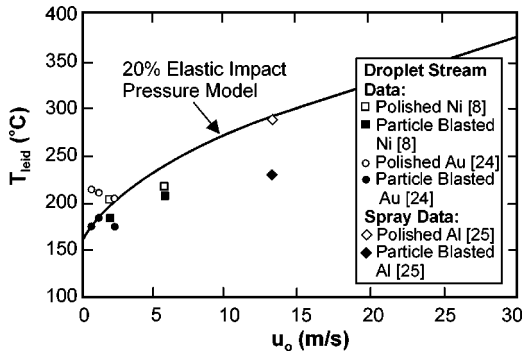

Fig. 5 Effect of surface roughness on the LFP for water droplets impinging upon metallic surfaces as determined experimentally and compared with the LFP model for a polished aluminum surface. The uncertainties of experimental Leidenfrost temperatures and droplet impact velocities measured in studies [8,24,25] were reported not to exceed ±10°C and ±0.5 m/s, respectively.

interfacial impact pressure, and the Leidenfrost temperature is the focus of ongoing studies in an effort to broaden and enhance the prediction capabilities of the current LFP model.

Conclusions

The present study employed an existing LFP model for sessile drops [3], and extended its capability to include impinging drops and sprays. The previous model, which was constructed around vapor bubble kinetics and surface cavity size characterization, was expanded to account for the sharp pressure rise that occurs at the liquid-solid interface during droplet impact. Upon evaluation of the current LFP model with an experimental database for droplets and sprays, the following key conclusions were drawn:

1. The Leidenfrost temperature for a droplet impinging upon a heated surface is highly dependent on the impact velocity. The model developed in this study successfully captured this velocity dependence.
2. The physical processes that govern the LFP of sessile drops are similar to those for impinging drops. The primary difference in the LFP predictions for sessile drops and impinging drops, is the evaluation of the liquid properties at the liquid-solid interface. For impinging drops, the sharp pressure rise that occurs at the liquid-solid interface during impact, must be accounted for so that the fluid properties can be accurately predicted.
3. This study revealed that the 20 percent elastic impact pressure model [18,19] is adequate for predicting the liquid properties of impinging drops at the liquid-solid interface.
4. The present LFP model was substantiated with experimental data for water drops impinging on a surface where the roughness feature sizes were of the same order of magnitude as the bubble nucleation cavities. Additional empirical data revealed that for rougher surfaces, the model predicts an upper bound of the Leidenfrost temperature.

Nomenclature

Symbol

$AB\%$ = percent liquid-solid interface area coverage by vapor
a_1, a_2 = coefficients in cavity size distribution
c_p = specific heat at constant pressure
h_{fg} = latent heat of vaporization
k = thermal conductivity
n = number of surface cavities per unit area per unit interval (sites $\mu m^{-2}\,\mu m^{-1}$)
nc = cumulative number of surface cavities per unit area (sites μm^{-2})
nc_a = cumulative number of active surface cavities per unit area (sites μm^{-2})
P = pressure
Q'' = volumetric spray flux ($m^3\,s^{-1}\,m^{-2}$)
R = bubble radius
$\dot{R}$ = first derivative of bubble radius with respect to time
$\ddot{R}$ = second derivative of bubble radius with respect to time
r = surface cavity radius
r_a = radius of active surface cavity (μm)
T = temperature
t = time
v_{fg} = specific volume difference between vapor and liquid
y = normal distance from solid surface

Greek Symbols

α = thermal diffusivity
$\Delta AB\%/\Delta t$ = average vapor layer growth rate
ΔT_{sat} = surface superheat, $T_s - T_{sat}$
ρ = density
σ = surface tension
ψ = fraction of cavities that participate in the vapor layer growth

Subscripts

a = active
f = liquid
g = vapor
i = liquid-solid interface
leid = Leidenfrost condition
max = maximum
min = minimum
o = initial, nucleation
s = surface, solid
sat = saturation
∞ = liquid condition far from bubble interface

References

[1] Bernardin, J. D., and Mudawar, I., 1995, "Use of the Quench Factor Technique to Predict Material Hardness in Heat Treatable Aluminum Alloys," Int. J. Heat Mass Transfer, **38**, pp. 863–873.
[2] Bernardin, J. D., and Mudawar, I., 1999, "The Leidenfrost Point: Experimental Study and Assessment of Existing Models," ASME J. Heat Transfer, **121**, pp. 894–903.
[3] Bernardin, J. D., and Mudawar, I., 2002, "A Cavity Activation and Bubble Growth Model of the Leidenfrost Point," ASME J. Heat Transfer, **124**, pp. 864–874.
[4] Yang, S. R., and Kim, R. H., 1988, "A Mathematical Model of the Pool Boiling Nucleation Site Density in Terms of the Surface Characteristics," Int. J. Heat Mass Transfer, **31**, pp. 1127–1135.
[5] Wang, C. H., and Dhir, V. K., 1993, "Effect of Surface Wettability on Active Nucleation Site Density During Pool Boiling of Water on a Vertical Surface," ASME J. Heat Transfer, **115**, pp. 659–669.
[6] Panton, R. L., 1984, *Incompressible Flow*, John Wiley & Sons, New York.
[7] Mikic, B. B., Rohsenow, W. M., and Griffith, P., 1970, "On Bubble Growth Rates," Int. J. Heat Mass Transfer, **13**, pp. 657–666.
[8] Bernardin, J. D., 1996, "Leidenfrost Point and Film Boiling Heat Transfer of Single Droplets and Sprays," Ph.D. thesis, Purdue University, West Lafayette, IN.
[9] Cole, R., and Shulman, H. L., 1965, "Bubble Growth Rates at High Jakob Numbers," Int. J. Heat Mass Transfer, **9**, pp. 1377–1390.
[10] Han, C. Y., and Griffith, P., 1965, "The Mechanism of Heat Transfer in Nucleate Pool Boiling-Part I," Int. J. Heat Mass Transfer, **8**, pp. 887–904.
[11] Johnson, Jr., M. A., De La Pena, J., and Mesler, R. B., 1966, "Bubble Shapes in Nucleate Boiling," American Institute of Chemical Engineers Journal, **12**, pp. 344–348.
[12] Carey, V. P., 1992, *Liquid-Vapor Phase-Change Phenomena: An Introduction to the Thermophysics of Vaporization and Condensation Processes in Heat Transfer Equipment*, Hemisphere, New York.
[13] Lee, H. S., and Merte, H., 1996, "Spherical Vapor Bubble Growth in Uniformly Superheated Liquids," Int. J. Heat Mass Transfer, **39**, pp. 2427–2447.

[14] Forster, H. K., and Zuber, N., 1954, ''Growth of a Vapor Bubble in a Superheated Liquid,'' J. Appl. Phys., **25**, pp. 474–478.
[15] Heymann, F. J., 1969, ''High-Speed Impact Between a Liquid Drop and a Solid Surface,'' J. Appl. Phys., **40**, pp. 5113–5122.
[16] Churchill, R. V., 1944, *Modern Operational Mathematics in Engineering*, McGraw-Hill, NY.
[17] Labeish, V. G., 1994, ''Thermodynamic Study of a Drop Impact against a Heated Surface,'' Exp. Thermal Fluid Sci., **8**, pp. 181–194.
[18] Engel, O. G., 1955, ''Waterdrop Collisions with Solid Surfaces,'' J. Research National Bureau Standards, **54**, pp. 281–298.
[19] Engel, O. G., 1960, ''Note on Particle Velocity in Collisions between Liquid Drops and Solids,'' J. Research National Bureau Standards-A. Phys. Chem., **64A**, pp. 497–498.
[20] Bankoff, S. G., and Mikesell, R. D., 1959, ''Bubble Growth Rates in Highly Subcooled Nucleate Boiling,'' Chem. Eng. Prog. Symp. Series, **55**, pp. 95–102.
[21] Hsu, Y. Y., 1962, ''On the Size Range of Active Nucleation Cavities on a Heating Surface,'' ASME J. Heat Transfer, **84**, pp. 207–213.
[22] Clark, H. B., Strenge, P. S., and Westwater, J. W., 1959, ''Active Sites for Nucleate Boiling,'' Chem. Eng. Prog. Symp., **55**, pp. 103–110.
[23] Klinzing, W. P., Rozzi, J. C., and Mudawar, I., 1992, ''Film and Transition Boiling Correlations for Quenching of Hot Surfaces with Water Sprays,'' J. Heat Treating, **9**, pp. 91–103.
[24] Bernardin, J. D., Stebbins, C. J., and Mudawar, I., 1997, ''Effects of Surface Roughness on Water Droplet Impact History and Heat Transfer Regimes,'' Int. J. Heat Mass Transfer, **40**, pp. 73–88.
[25] Bernardin, J. D., and Mudawar, I., 1996, ''An Experimental Investigation into the Relationship between Temperature-time and Surface Roughness in the Spray Quenching of Aluminum Parts,'' ASME J. Eng. Mater. Technol., **118**, pp. 127–134.
[26] Bernardin, J. D., 1993, ''Intelligent Heat Treatment of Aluminum Alloys: Material, Surface Roughness, and Droplet-Surface Interaction Characteristics,'' Masters thesis, Purdue University, West Lafayette, IN.